



Design and Application of a Test Rig for Stationary Component Performance Measurement of Centrifugal Compressors

K. Zhao^{1,2}, Y. Liu¹, Y. Zhang^{2†}, X. Liu² and H. Shi²

¹ School of Energy and Power Engineering, Dalian University of Technology, Dalian, Liaoning, 116024, China

² Shenyang Blower Group Co., Ltd, Shenyang, Liaoning, 110869, China

†Corresponding Author Email: zhangy@shengu.com.cn

ABSTRACT

Experimental testing is an important method for studying centrifugal compressors. However, test rigs with rotating impellers are costly in terms of construction and operating expenses. To address this issue, this study introduces a stationary component performance test rig for centrifugal compressors using an existing wind tunnel. The rig comprises a blower to supply compressed air, a wind tunnel, and a test section of stationary centrifugal compressor model stage. Specially designed stationary guide vanes substitute the impeller to simulate the impeller outlet flow field. Flow field parameters are measured at the inlet and outlet of each model-scale stationary component using a five-hole probe. Measured results can be used to evaluate the performance of each stationary component. Comparison between measured data and CFD results reveals that the measurement results are in good agreement with CFD results. This validates the reliability of the built test rig and measurement. Afterwards an improved diffuser and return channel of the same centrifugal compressor model stage is tested. The experimental results show a 4% reduction in total pressure loss coefficient and a 1% increase in static pressure recovery coefficient compared to the original structure. These results align with the findings obtained on a rotating test rig, indicating the feasibility of the proposed stationary component aerodynamic performance test rig.

Article History

Received May 7, 2024

Revised October 21, 2024

Accepted October 29, 2024

Available online February 4, 2025

Keywords:

Centrifugal Compressors

Stationary Components

High Flow Coefficient

Stationary Guide Vanes

Experimental Test

1. INTRODUCTION

Centrifugal compressors are commonly used in industrial applications, and they typically have a single-shaft, multi-stage design. Each stage comprises a rotating centrifugal impeller and stationary components, such as a diffuser and a return passage (U-bend, return channel, and L-bend). Stationary components serve to eliminate the turbulence created by the rotating impeller and ensure uniform inlet conditions for the next stage. Although a single impeller efficiency has reached 96% (Sorokes, 2013), achieving further efficiency improvements is challenging. Aalburg et al. (2011) noted that the stationary component loss accounts for approximately 5–10% of the total machine loss, and the stationary components play a vital role in the overall efficiency and operating range of the machine. The efficiency of the machine is improved by optimizing the stationary components. Therefore, an in-depth study of the stationary components' internal loss mechanism is worthwhile.

In recent years, a significant increase has been observed in stationary components. The research methods mainly focus on numerical simulation and experimental measurement. Numerical simulation plays a vital role in the design process due to valuable guidance to designers (Lenke & Simon, 1999; Ferrara et al., 2004; Oh et al., 2005; Hildebrandt, 2011). Besides the advantages of numerical simulation, it still relies on experimental results to verify its accuracy (Seki et al., 2006; Gilarranz et al., 2009; Yagi et al., 2015; Rube et al., 2016). In new stationary member structure study, prediction of the actual flow use of numerical simulation methods is uncertain and not accurate. Therefore, experimental measurements and validation are required. However, conducting measurements on a rotating test rig is time-consuming and resource-intensive and poses safety risks.

In axial turbines, the plane cascade experiment has long been used as an economical and effective alternative to the rotational experiment. However, unlike axial turbines, the axial and radial sections of centrifugal compressors make experimental study impossible using

NOMENCLATURE			
b	width of passage	ζ	loss coefficient
c_p	static pressure recovery coefficient	η_{pol}	polytropic efficiency
D	pressure coefficient	φ	flow coefficient
Ma	Mach number	0	stationary guide vanes inlet
MP	Measurement Plane	1	impeller outlet
Mu	machine Mach number	2	diffuser outlet
N	design speed	3	return channel inlet
P	static pressure	4	L-bend outlet
P_t	total pressure	dif	diffuser
V_m	meridional velocity	im	impeller
V_t	tangential velocity	IN	stage inlet
Z	number of blades	OUT	stage outlet
α	flow angle	re	return channel
ε	total pressure ratio		

plane cascades. Despite this, researchers are still finding a way to apply this method. [Simpson et al. \(2008\)](#) carried out experimental measurements on a test rig containing a stationary component with a quarter of the return channel of a centrifugal compressor. They compared results with those from a rotating test rig to validate feasibility. The stationary test rig was then used to experimentally investigate the return channel blades ([Simpson et al., 2014](#)), employing a high-pressure gas that suppresses the suction-side secondary flow and enhances overall machine performance. [Aalburg et al. \(2008\)](#) introduced a pseudo-stage swirl blade group in front of the impeller to simulate the internal flow of a multistage compressor. [Xi et al. \(2019\)](#) followed the same to check the effect of the Reynolds number on the internal losses of the bend and return. [Aalburg et al. \(2011\)](#) designed a centrifugal compressor stationary component test rig with a flow coefficient of 0.12, exploring diffuser variations to reduce the radial dimension of the machine while maintaining efficiency. [Dolle et al. \(2019\)](#) performed flow measurements in the bend and return channel of a similar compressor, using a stationary component test rig for experimental measurements and optimizing their turbulence models with simulated data.

The stationary component test stand offers several advantages over its rotating counterpart. First, it allows for experimental components to be designed and fabricated at a reduced cost while significantly enhancing safety. Second, the stable experimental environment facilitates precise probe placement or optical flow field measurements (PIV or LDA), enabling the calibration of numerical models. Third, by adjusting the relative position of the static vane and the diffuser, the interaction between the static vane and the rotating vane can be approximated. This enables the stationary component test rig to serve as a bridge between numerical simulation results and rotational experimental measurements, reducing errors and validating predictions of the internal flow state and aerodynamic performance of fixed components under various operating conditions. Consequently, the stationary component test stand facilitates rapid screening of new fixed component structures and minimizes the safety risks of rotational experimental measurements.

The above literature review shows centrifugal compressors tested on stationary test rigs at low flow

coefficients and no research on high flow coefficients. A high flow coefficient compressor typically has a design flow coefficient of 0.15 or higher and operates at a machine Mach number exceeding 0.8. This requires a big test facility. This paper introduces the design and construction of a static test rig for a compressor with flow coefficient of 0.2 and its application. First the design principle of static guide vane (SGV) to replace the rotating impeller is elucidated. The use of the SGV results in a reduction in construction and experimental costs. Subsequently, five measurement planes in the static test rig, as well as the measurement mechanism and equipment, are introduced. Thereafter, the performance of each component is tested. Finally, the static test rig is employed to verify the performance of optimized static components for the same compressor stage.

2. DESIGN FOR STATIONARY COMPONENT TEST RIG

The performance of stationary components is assessed using a test rig with stationary guide vanes (SGVs) instead of rotating impellers, operating under real conditions. A continuous wind tunnel generates airflow through the model stage. Five-hole probes are employed to measure flow parameters at the inlet and outlet sections of each stationary component, providing data on total pressure, static pressure, velocity magnitude, and flow direction at various points. Aerodynamic performance is evaluated from these measurements, providing theoretical support for the design and optimization of the model stage.

The stationary component performance test rig is accommodated within a wind tunnel (Fig. 1), powered by a 350 kW fan providing a maximum flow rate of 12.5 m³/s and a maximum absolute pressure of 1.2 bar. The flow rate at the inlet of the test section is regulated by adjusting three valve openings. A honeycomb structure is installed in the settling chamber upstream of the test section to break large vortices into smaller ones, complemented by two gauzes to further reduce the remaining small vortices. The resulting uniform flow enters the test section via a converging section. Exiting the test section, airflow passes through a diffuser and a muffler before being released into the atmosphere.

The prototype centrifugal compressor in the test

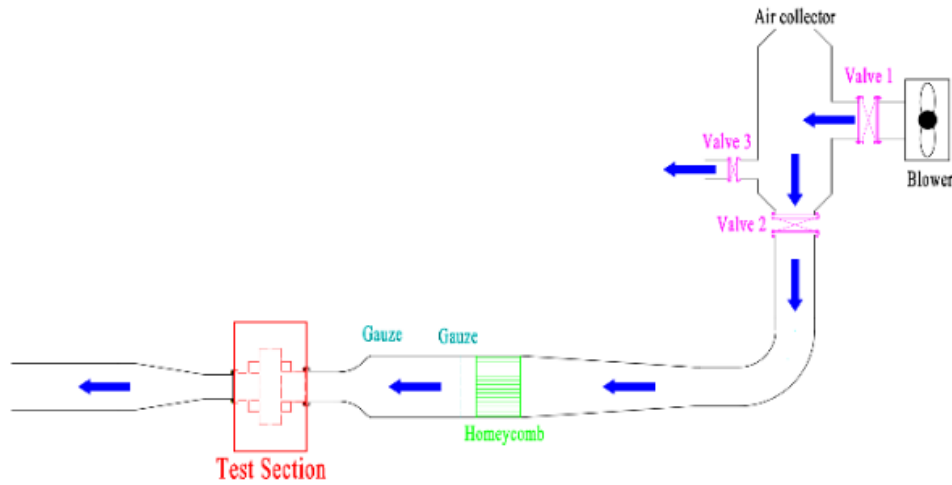


Fig. 1 Schematic diagram of the wind tunnel test rig

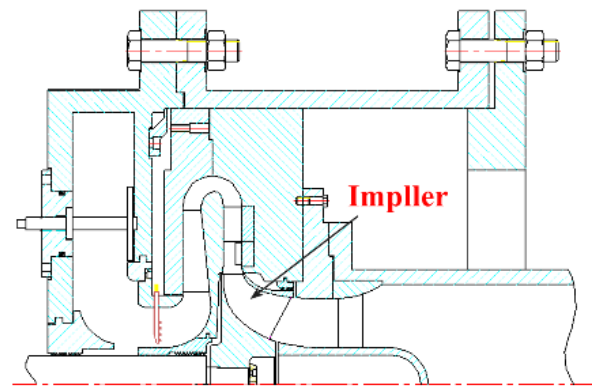
Table 1 Main geometric parameters and design conditions

Geometric parameters	Symbol	Value
Design mass flow coefficient	ϕ	0.2
Design machine Mach number	Mu_2	0.8
Design speed	n	11650
Number of impeller blades	Z_{im}	17
Number of diffuser blades	Z_{dif}	22+22
Number of return channel blades	Z_{re}	18
Impeller outlet diameter	D_2	450
Impeller outlet width	b_2	40

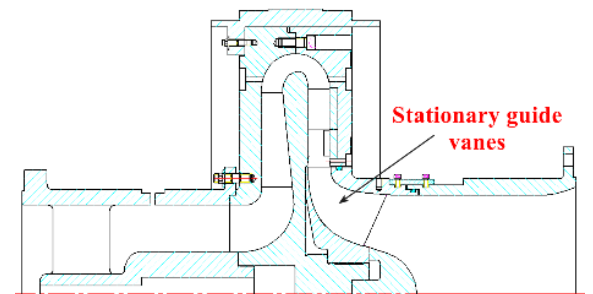
section represents the first stage of an industrial multistage centrifugal compressor, comprising a shrouded impeller, a diffuser, and a return channel. The key geometric parameters are detailed in Table 1.

Figure 2 illustrates a sectional view of the rotating and stationary test rigs. The rotating test rig, enclosed in a thick casing for safety, poses challenges for measurements. Due to structural constraints, measurement probes can only be placed at specific locations, such as the inlet and outlet, limiting detailed data collection and derivation to the overall performance curve of the centrifugal compressor. Additionally, it is difficult to perform 1:1 experimental measurements on the rotating test rig due to structural size limitations. Our previous research on a scaling study on this compressor employed a scaling factor of 0.8 (Zhao et al., 2017; Li et al., 2021). In contrast, the stationary component test rig is designed at full scale with a scaling factor of 1.0.

Figure 2 depicts that both test rigs feature axial inlet flow directions but diverge in their exhaust approaches. The rotating test rig employs a volute structure at the outlet, while the stationary component test rig adopts an axial pipe exhaust to measure the outlet flow field, aligning with the inlet flow method. While the internal structure of the test section in the stationary component test rig is identical to that of the rotating experimental test



(a) Rotating test rig



(b) Stationary test rig

Fig. 2 Comparison of the test rigs

rig, variations exist in the inlet impeller and the outlet structure. The stationary component test rig lacks a heavy casing, offering a stable test environment without rotating components.

Figure 3 illustrates the components of the test rig. The rotating impeller is substituted by fixed stationary vanes (Fig. 3(a)). The diffuser comprises a tandem blade diffuser (Fig. 3(b)), featuring a half-height splitter diffuser and a full-height diffuser in the first and second rows, respectively. These diffuser rows are machined individually and then embedded in dedicated slots in the



Fig. 3 Test rig components: (a) SGV; (b) tandem-blade diffuser; (c) return-channel blades; (d) test section; (e) overall structure

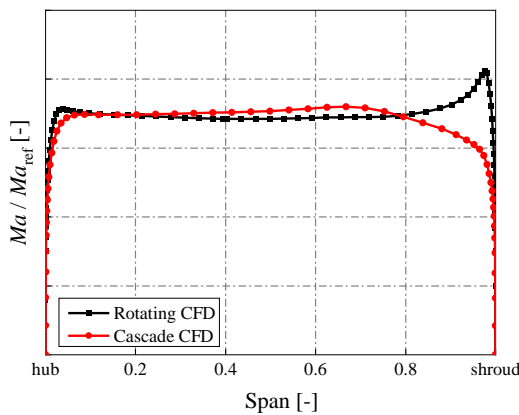
faceplate. The return blades (Fig. 3(c)) and the return channel are machined as a unified unit, encompassing the hub side of the entire stationary component and the return channel blades. They are affixed to the rear cover plate via bolt holes on the return channel vanes.

During assembly, the diffuser, bend, and return channel with vanes are integrated into a single component using front and rear cover plates. This assembled component is then mounted onto the test section using upper and lower bucket assemblies. Subsequently, the stationary vanes are assembled in the component. Rubber rings are incorporated at all joints of the test section components to prevent any leakage. The resulting test

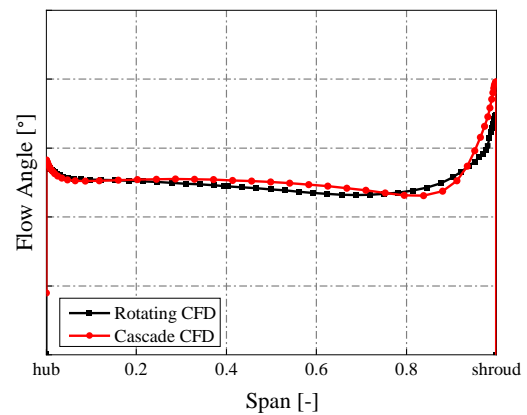
section is depicted in Fig. 3(d). All components utilized in this experiment are fabricated with metallic materials to ensure structural strength. The processing requirements are consistent with those of the rotating experimental test rig, resulting in a relatively heavy overall weight. This weight poses challenges during installation and debugging. Future work can focus on using additive manufacturing techniques to fabricate stationary components other than the fixed structure in sections, reducing the test cycle and the cost.

Figure 3(a) showcases the stationary vane, a pivotal component of the stationary component test rig. During design, the meridional distribution of the outlet flow field is matched to that of the actual impeller by adjusting the blade angle distribution. The impeller’s meridional structure and blade count remain unaltered. Figure 4 shows a comparison of the outlet flow field parameters of the stationary vanes and the rotating impeller, including the Mach number, flow angle, warp velocity, and tangential velocity.

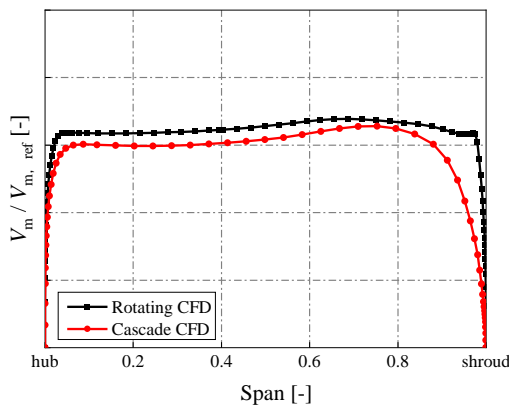
Figure 4 shows a good overall fit of parameters at the outlet of the stationary vanes and the rotating impeller. However, some discrepancies are observed on the disk and cover sides. These errors arise because stationary guide vanes do not affect the gas but rather deflect the airflow. Outlet vane velocity primarily depends on inlet velocity and the ratio of the inlet and outlet cross-sectional areas, with vane shape exerting minimal influence. To meet the outlet flow angle requirement, vanes on the cover side



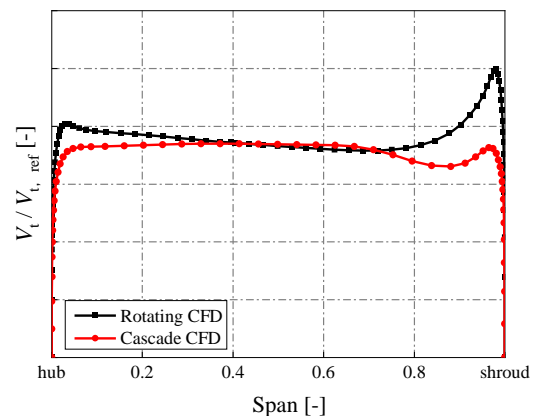
(a) Mach number



(b) Flow angle

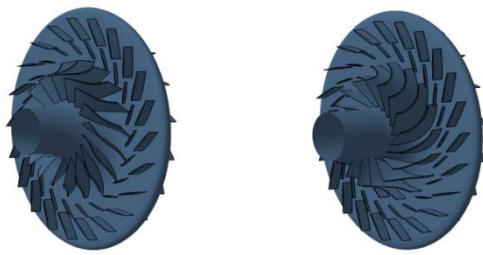


(c) Meridional velocity



(d) Tangential velocity

Fig. 4 Comparison of design parameters of SGV



(a) Rotating impeller (b) SGV

Fig. 5 Comparison of impeller and SGV

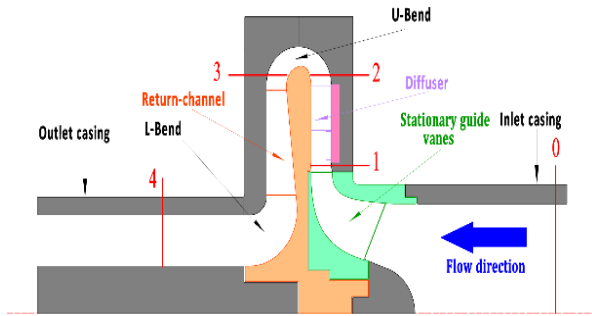


Fig. 6 Schematic diagram of measurement sections on the stationary components experimental test rig

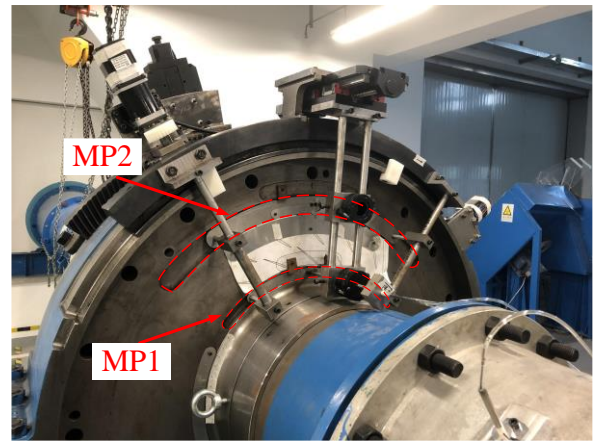
feature a large radius of curvature, causing gas to separate from the wall and resulting in reduced overall velocity on the cover side. Following the requirements of Mach number and flow angle, the stationary vanes are developed to meet the design criteria, prioritizing flow angle while also considering the Mach number. Figure 5 depicts the structure of the designed stationary vanes and the original rotating impeller.

3. MEASURING POSITION AND MEASURING EQUIPMENT

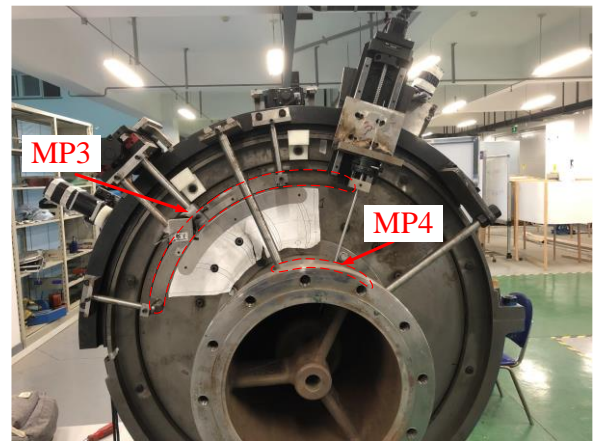
Unlike conventional rotating test rigs, the stationary component test rig offers greater instrumentation capabilities. Figure 6 showcases five measurement sections, each capable of accommodating multiple measurement instruments.

At measurement plane 0 (MP0), four static pressure taps are evenly distributed around the pipe wall circumference to gauge wall static pressure. A total pressure probe and a total temperature probe are positioned between two adjacent static pressure taps. The inlet flow angle distribution and turbulence intensity of the test section are measured by installing a five-hole probe or a hot-wire probe that can move radially at the position of the total pressure probe.

Measurement plane 1 (MP1) is situated at the outlet of the stationary vanes, corresponding to the diffuser inlet (Fig. 7(a)). In section 1, a five-hole probe is located, which can move both spanwise and circumferentially. The measurement angle in the circumferential direction is 1.5 blade pitches, encompassing a complete flow passage. To maintain a uniform distribution of measurement points, 18



(a) Sections 1 & 2



(b) Sections 3 & 4

Fig.7 Measurement locations

points are positioned in the spanwise direction and 49 points in the circumferential direction, totaling 18×49 measurement points.

Measurement plane 2 (MP2) is located at the outlet of the diffuser, serving as the inlet of the U-bend (Fig. 7(a)). The location of the measurement points is identical to that of section 1. Measurement plane 3 (MP3) is located at the inlet of the return channel, which is the outlet of the U-bend (Fig. 7(b)). Its radial position and measurement point arrangement are identical to those of section 2.

Measurement plane 4 (MP4) is positioned at the outlet section, at 1.5 times the radial height from the outlet of the L-bend (Fig. 7(b)). A total of 49×27 measurement points are organized circumferentially and radially. Four static pressure probes are evenly distributed along the circumference at 0.5 times the outlet height downstream of section 4. Each measurement point in all measurement sections is measured for 10 s, obtaining 400 sets of data.

Almost 4000 measurement points span across the four measurement sections, making the entire experimental measurement a time-intensive process. The probes in sections 1 and 2 are on the same trajectory, while those in sections 3 and 4 are on a different path, halving the measurement time. However, a standard measurement process consumes about 9 h, comprising 1 h for equipment stabilization and 8 h for data acquisition. Despite the

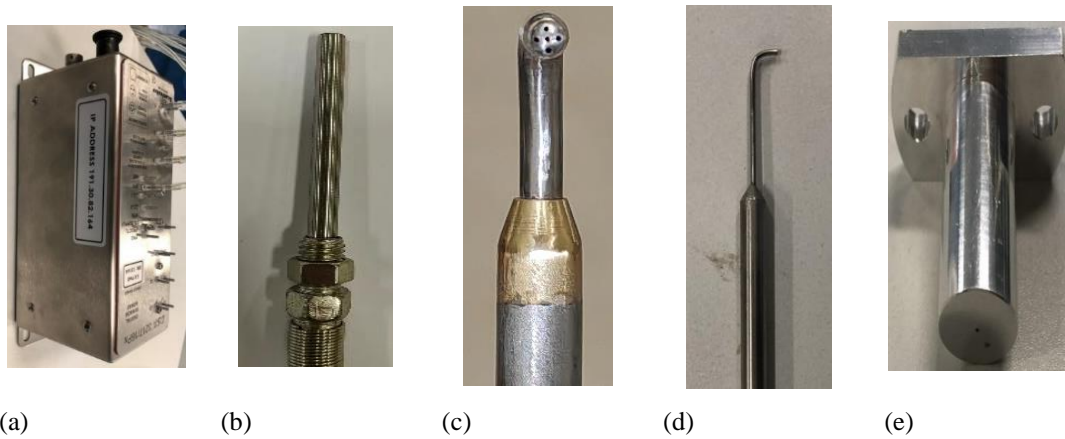


Fig. 8 Measurement equipment: (a) DSA3217; (b) total temperature probe; (c) five-hole probe; (d) total pressure probe; (e) static pressure probe

warm-up process, inlet conditions experience drift, with an average variation of 200 Pa in inlet pressure throughout the test duration. While this pressure drift is largely compensated for in the loss computations, it results in an associated error of approximately 0.5%.

All pressures are measured using a Scanivalve DSA3217 pressure scanner with 16 differential pressure transducers (Fig. 8(a)). The module's measuring range is 5 psi, with an accuracy of $\pm 0.05\%$ FS in pressure measurements. The experiment employs a thermocouple model of Pt100 platinum resistance thermometer (Fig. 8(b)), with a measurement range of -50°C to 300°C and an accuracy level of 1°C . The actual accuracy is within $\pm 1^{\circ}\text{C}$, considering the sensor heat transfer error and some system errors. All five-hole probes (Fig. 8(c)) are calibrated, with the measurement angle error within $\pm 0.5^{\circ}$. However, the experimental measurement angle error is within $\pm 1^{\circ}$, considering the installation and calibration errors. The calibration error of total pressure and static pressure measured by the five-hole probe is 0.05%. The total pressure probe (Fig. 8(d)) maintains an accuracy of 99.7% within $\pm 5^{\circ}$ during calibration. Under installation situations, the pressure measured by the total pressure probe is considered the actual total pressure. In addition, the static pressure probe is calibrated in accordance with the experimental requirements.

4. VERIFICATION OF THE STATIONARY COMPONENT TEST RIG

The stationary component test rig is incorporated into the wind tunnel featuring a 90° bend preceding the main test section (Fig. 3). To enhance flow field uniformity at the inlet of the test section and mitigate the bend's influence, honeycombs and gauzes are placed in the force dissipation section. At the entrance of the test section (section 0), a five-hole probe mounted on the stepper motor is employed to measure the yaw and pitch angle distribution of the airflow (Fig. 9). The results indicate the uniformity of the flow in the tube and the elimination of residual swirl of the airflow in the upper 90° curve. The yaw and pitch angles of the central main flow area (80% of the flow channel) are below 1° . The flow angle variation in the boundary

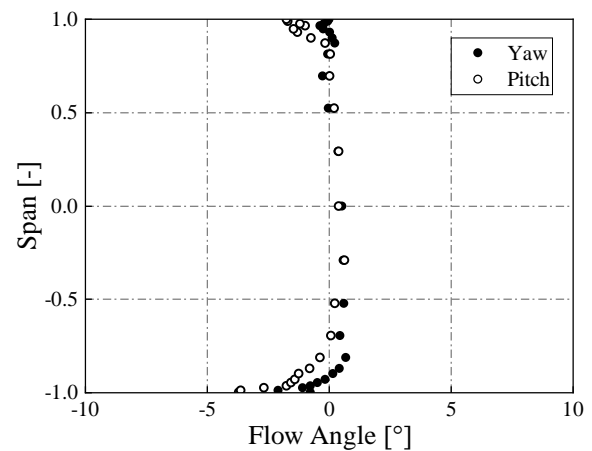
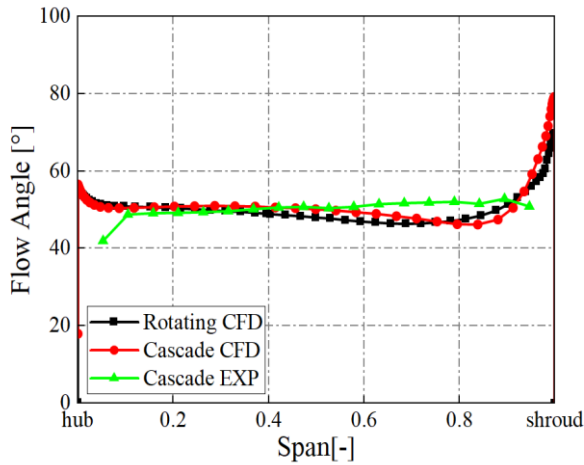


Fig. 9 Yaw and pitch angle distributions at the inlet of the test section (MP0)

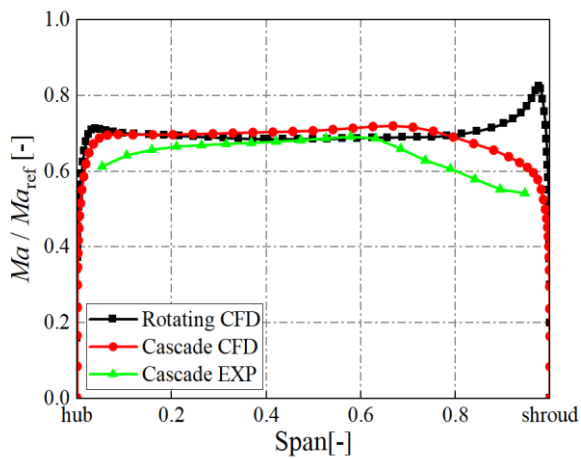
layer near the wall is below 2° . The test results reveal that the inlet air flow is uniform, ensuring no impact with subsequent experimental measurements.

The stationary vanes are a pivotal element of the stationary component test rig for centrifugal compressors. The blade angle distribution of the original rotating impeller is adjusted to match the spanwise distribution of the outlet Mach number and flow angle of the actual impeller outlet while keeping the number of blades or meridional flow path shape unchanged.

Figure 10 illustrates a comparison between the circumferentially averaged yaw angle and Mach number distributions along the span at the outlet of the stationary vanes, serving as the inlet of the diffuser (MP1), obtained from experimental and numerical simulations. This study proposes a novel experimental test rig for stationary components. The numerical computation approach is described in our previously published studies (Zhao et al., 2017; Li et al., 2021). Safety considerations and structural constraints of the rotating test rig precluded the placement of probes at the impeller outlet. This limitation arises from the scaled-down dimensions of the rotating test rig (0.8 times the actual size) and the narrow gap (16 mm) between the trailing edge of the impeller and the leading edge of



(a) Flow yaw angle



(b) Mach number

Fig. 10 Comparison of the spanwise distributions of the circumferentially averaged Mach number and flow yaw angle at the outlet of the stationary guide vanes

the tandem diffuser. Figure 10(a) indicates consistent overall trends in experimental and simulated flow yaw angles, with significant differences only observed on the cover side. Figure 10(b) reveals that the Mach numbers of the stationary vanes and the rotating impeller have similar variation trends and numerical values when the blade height is below 60% but diverge completely on the cover side. This discrepancy arises because the stationary vanes redirect the airflow without impacting the gas directly. The outlet velocity of the guide vanes is primarily governed by the inlet velocity and the ratio of inlet and outlet cross-sectional areas and is not significantly influenced by the shape of the guide vanes. To achieve the desired outlet flow angle, cover side vanes feature a small radius of curvature, causing gas separation from the wall and reducing the overall velocity on the cover side of the stationary vanes.

In actual operations, the relative position between the impeller and the diffuser is dynamic. Therefore, the flow field at the diffuser inlet is assumed to be uniform in the circumferential direction. However, in the stationary



Fig. 11 Actual relative position between stationary guide vanes and diffuser

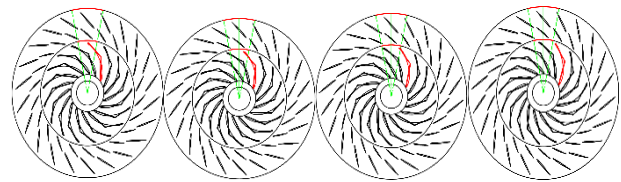


Fig. 12 Relative position between stationary guide vanes and diffuser at 0°, 5.3°, 10.6°, and 15.9°

component test rig, the stationary vanes substitute the rotating impeller. The relative position between the trailing edge of the stationary vanes and the leading edge of the diffuser is fixed. Figure 11 illustrates the relative position change between the stationary vanes and the tandem blade diffuser during installation. Consequently, the flow field at the MP1 undergoes variation with the circumferential position of the stationary vanes when the measurement position is fixed, influencing the actual flow field at the subsequent test sections. An experimental investigation was conducted with the stationary vanes in various positions.

The stationary guide comprises 17 vanes, with each channel approximately 21.2°. At the vanes' outlet, each channel is divided into four components, roughly 5.3° each. A chosen vane is rotated clockwise to four different positions: 0°, 5.3°, 10.6°, and 15.9°. Figure 12 depicts the relative position graph, with the selected guide vanes as red blades. Two concentric arcs (highlighted in red) delineate the circumferential measurement ranges of the probes at MP1 and MP2.

Figures 13–15 show a comparison of numerical computations and experimental measurements of four angles at the MP1. The plotted area encompasses a full pitch, with the five-hole's spanwise displacement ranging from 5% to 95% of the radial height. It can be observed that there is a discrepancy between the numerical simulation results and the experimental results in the three figures. This discrepancy can be attributed to the fact that the measured section is defined by the center line of the probe rod, whereas there is a certain distance between the

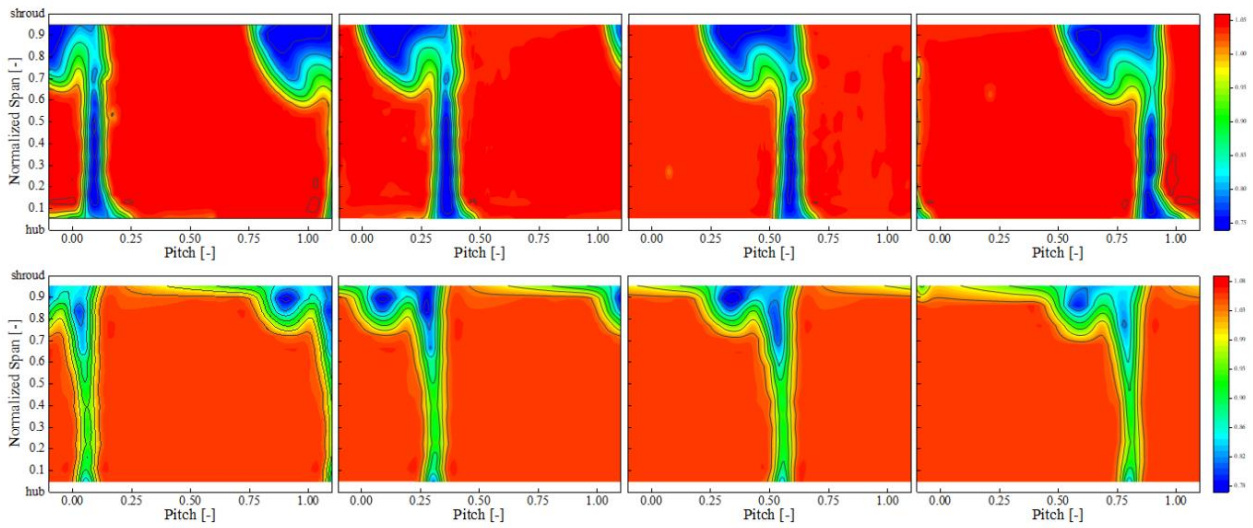


Fig. 13 Comparison of total pressure at MP1 (top: experiment, bottom: CFD)

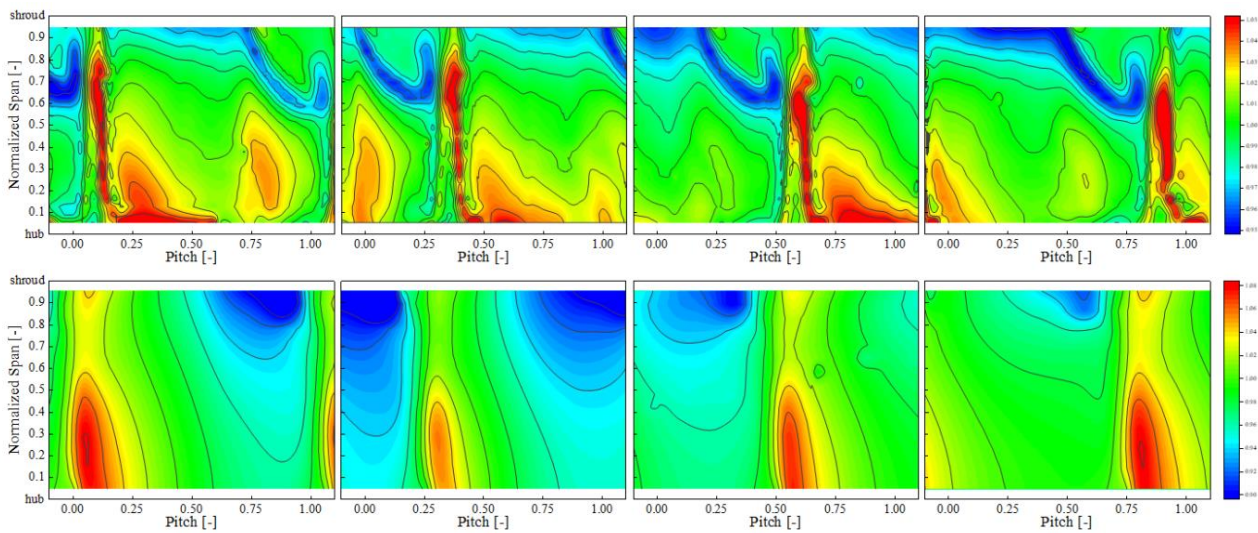


Fig. 14 Comparison of static pressure at MP1 (top: experiment, bottom: CFD)

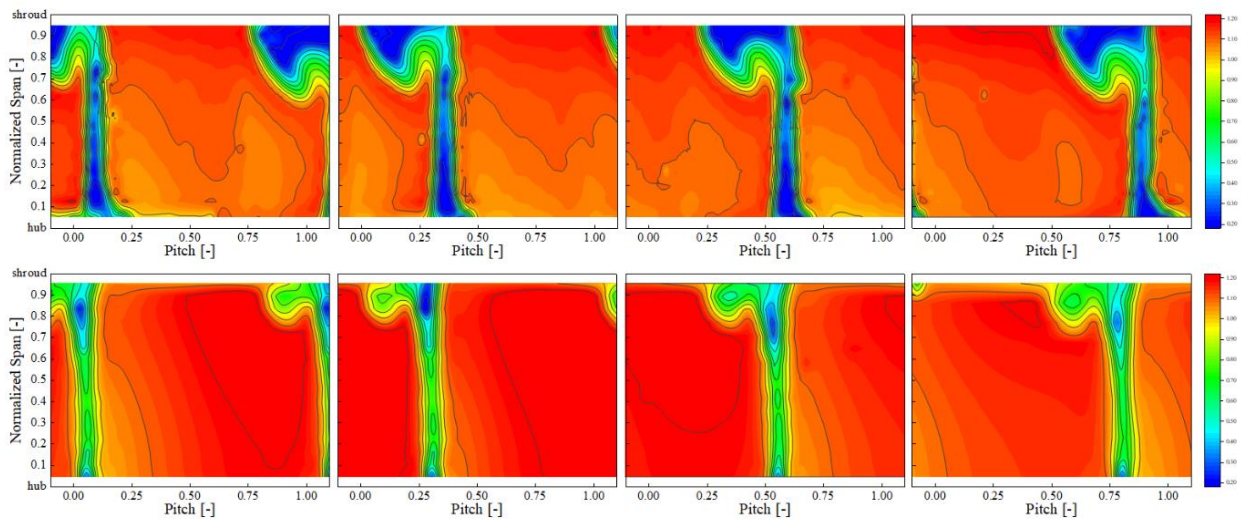


Fig. 15 Comparison of Mach number at MP1 (top: experiment, bottom: CFD)

probe head and the center line of the probe rod. This distance results in a discrepancy between the actual measured section and the theoretical section. However, when the data is processed, the data within a pitch is selected and averaged. Consequently, the discrepancies between experimental results and simulations have minimal influence on the overall outcome.

Figure 13 reveals that the simulated and experimental values have consistent overall variation trends. A trailing vortex forms at the guide vanes' trailing edge, while a substantial separation vortex emerges at the cover's suction side, with its size and intensity exceeding the simulated values significantly. This discrepancy arises because the simulation uses an adiabatic and smooth wall boundary condition where the working fluid is an ideal gas. However, the real impeller, though polished, retains roughness due to welding and environmental factors, such as humidity. Long-term experiments cause the wall surface to rust, further increasing its roughness. The expanded separation vortex yields a larger low-speed region on the canopy's suction side, resulting in a circumferentially averaged Mach number at the outlet of the vane cascade that is much lower than the simulated value, as shown in the Mach number contour of Fig. 15.

Figure 14 illustrates the comparison of static pressure contours at the four measurement angles. Unlike the total pressure contour (Fig. 13) and the Mach number contour (Fig. 15), the static pressure contour does not fit well between the numerical and experimental results. In the

experimental measurement contour, discontinuous islands of static pressure distribution are evident on the pressure and suction sides near the blade's hub side. This phenomenon stems from the distribution pattern of measurement points during the measurement, with 18×49 points and gaps between them at the MP1. Therefore, significant differences can arise between data from any two points, causing the contour to appear as discontinuous islands. Conversely, numerical results exhibit continuous contours without gaps, depicting a continuous static pressure distribution. A notable difference exists between the blade's suction side and the numerical results. The numerical contour features a continuous low-pressure region, while the experimental contour showcases only a ring of low pressure at the outer edge. This discrepancy arises from the flow angle of the recirculation zone at this location exceeding the calibration range of the five-hole probe used ($\pm 30^\circ$). Despite errors between experimental and numerical results of the static pressure contour, their distribution patterns remain consistent. The actual flow field is not as shown in the experimental contour, and the guide effect of the stationary guide vanes can still function normally.

Figure 16 presents the average values of total pressure, static pressure, Mach number, and flow angle for the remaining three sections measured at four positions of the stationary vanes (0° , 5.3° , 10.6° , and 15.9°), in addition to section MP1. In the figure, the horizontal coordinates signify the measurement sections MP1, MP2, MP3, and MP4. A channel is created for each

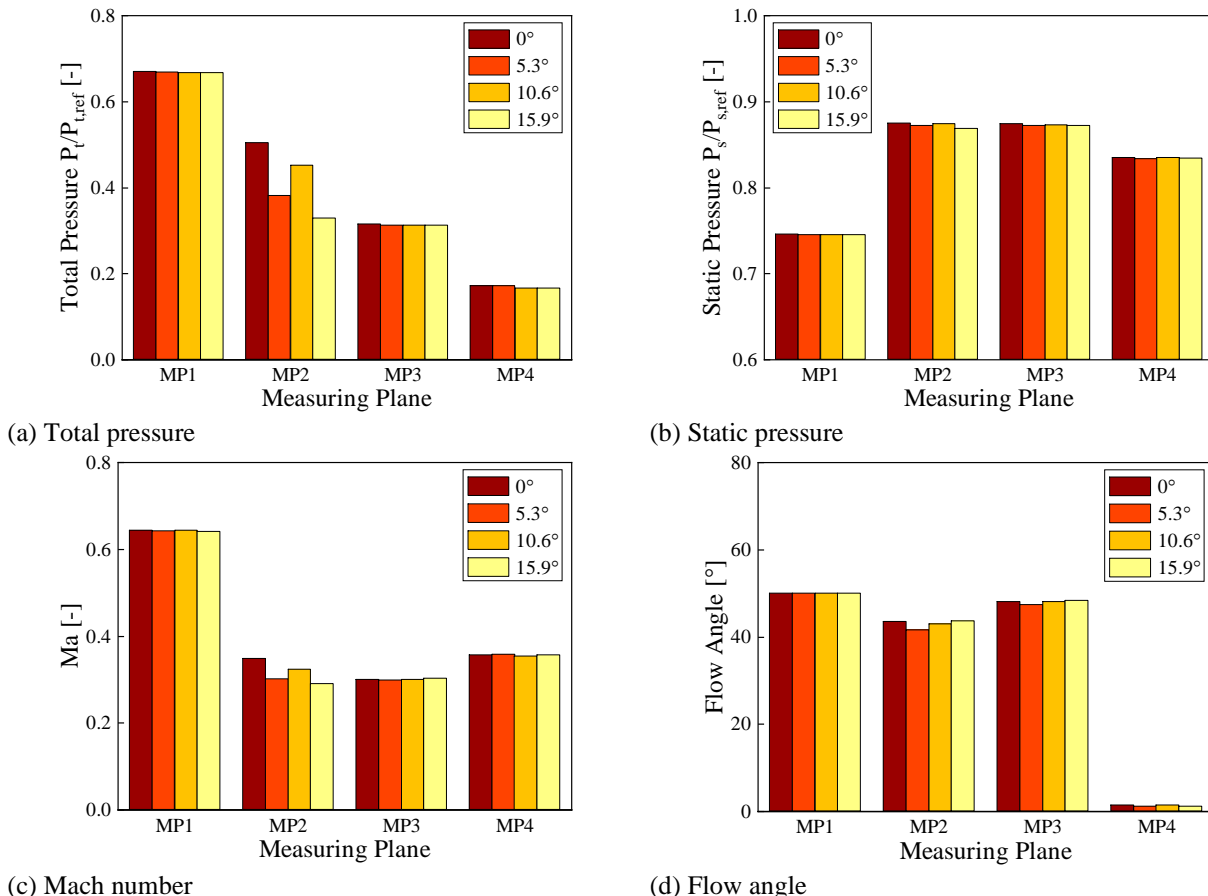


Fig. 16 Average parameters of each section at different angles

section, to measure angles based on the number of blades. The average of the selected data represents the area average of the corresponding section.

Figure 16 shows the consistent parameters of the MP1 despite variations in stationary blade angles, primarily influenced by weather changes (Figs. 13–15). Each section requires about 4 h for measurement, with simultaneous measurement of two sections feasible using a specially designed mechanism, totaling 8 h for all four sections at a single angle. Minor fluctuations in atmospheric pressure and temperature may occur, impacting flow rate consistency. In order to minimize the influence of meteorological conditions on the test results, dimensionless processing for the measurement data is carried out. Significant parameter variations are observed in the MP2, particularly at the diffuser outlet section, with consistent trends in total pressure, static pressure, and Mach number. The impact of changing the stationary vane angle is evident. Each rotation of the stationary vane causes a corresponding change in the position of the trailing vortex it generates, resulting in a change in the flow field at the diffuser inlet. However, measurements at the diffuser outlet remain constant despite vane rotations, resulting in varied data readings. The average parameter values for the MP3 and MP4 are identical, indicating negligible angle-induced flow field alterations in these two sections. This effect is nullified in the bend and the return. Consequently, the flow fields of each section measured at different positions of the stationary vanes represent a specific moment during the actual flow. Exploring the flow in the stationary components of the centrifugal compressor at this moment can offer insights unattainable through rotating experimental test rigs.

To evaluate the aerodynamic performance of the centrifugal compressor, the total pressure loss coefficient and static pressure recovery coefficient are employed, as shown with parameters denoting the average values of the four angles measured at each section.

Static pressure recovery coefficient:

$$c_p = \frac{P_{OUT} - P_{IN}}{P_{t,IN} - P_{IN}}$$

Total pressure loss coefficient:

$$\zeta = \frac{P_{t,IN} - P_{t,OUT}}{P_{t,IN} - P_{IN}}$$

Figure 17 shows a comparison of the specific pressure recovery coefficients of each stationary component. The total pressure loss coefficients are also compared in Fig. 18 using the same approach.

Figure 17 presents the minimal errors between the experimental measurements and numerical simulations of static pressure recovery coefficients, with consistent variation trends reflecting actual conditions. Static pressure increases predominantly occur in the diffuser, while the static pressure remains relatively unchanged in the bend and decreases in the return channel. However, Fig. 18 reveals a substantially higher disparity in total pressure loss coefficients between numerical and experimental results. The discrepancy can be attributed to

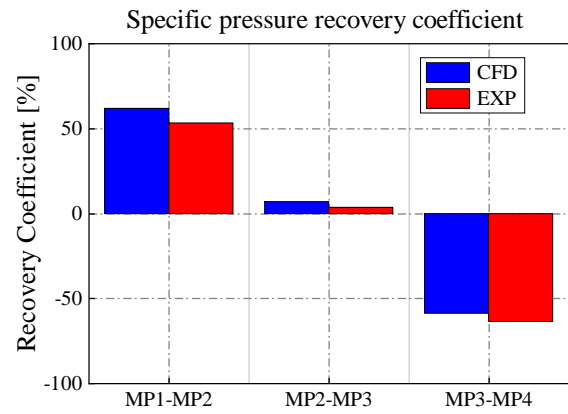


Fig. 17 Comparison of static pressure recovery coefficients

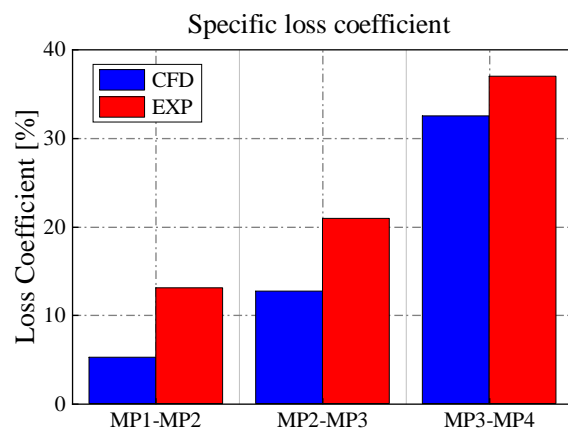


Fig. 18 Comparison of total pressure loss coefficient

the outlet flow field (MP1) of the stationary guide vane. As illustrated in Figures 10 and 13-15, there is a significant discrepancy in the MP1. The reasons for this have been explained in the previous section. The discrepancy in the flow field within the MP1 has resulted in a significant disparity between the actual measurement result and the numerical simulation result for the vaneless diffuser (MP1-MP2). This non-uniformity in the flow within the vaneless diffuser persists in the U-bend (MP2-MP3), which is a contributing factor to the considerable difference observed in the loss coefficient. In the MP3-MP4, the difference is relatively small, indicating that the inhomogeneity of the return-channel inlet is close to the numerical simulation results.

The gas flow undergoes a 180° directional change at the diffuser outlet (MP2) post-bend passage, inducing mixing. Real-world conditions entail higher turbulence intensity into the bend, resulting in increased velocity gradient and more pronounced mixing, escalating losses. At the bend exit (MP3), flow field alterations due to stationary vane rotation are significantly mitigated. Minor parameter variations across angles indicate the superiority of the selected bend structure in achieving flow field uniformity, as demonstrated in the MP3 of Fig. 16. The enhancement in the flow field due to the bend results in

simulated total pressure loss values in the return channel that closely match the experimental values.

When the inlet flow field of the stationary components is uniform, the experimental measurements align well with the numerical simulations, aided by variations in the static pressure recovery coefficient. This mechanism eliminates machining errors from surface roughness and welding chamfers of the stationary guide vanes. The stationary component test rig validates the performance of the diffuser, bend, and return duct. In the future, additive manufacturing can be employed for processing and manufacturing stationary components.

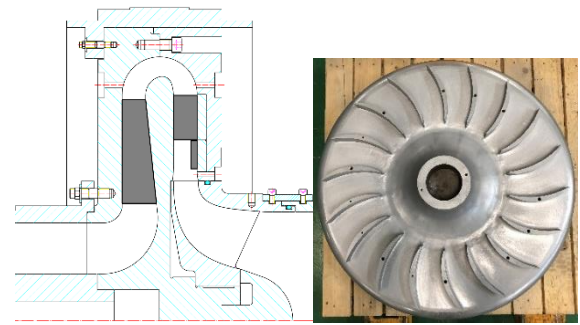
The stationary component test rig generates an outlet flow field akin to a rotating impeller. Flow conditions, such as flow angle and Mach number, are consistent with the corresponding outlet conditions of the rotating impeller, meeting design requirements. However, it is essential to note that the flow conditions near the casing may be different.

5. STRUCTURE OPTIMIZATION

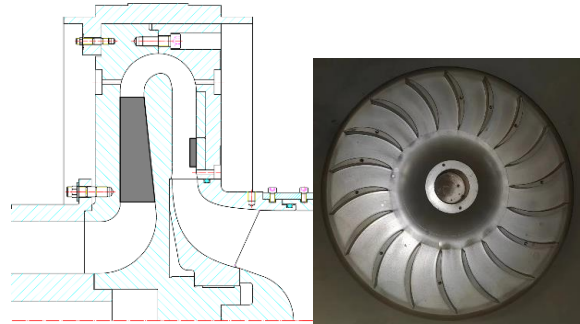
In our previous study, we optimized the structure of stationary components while maintaining the impeller shape and meridional flow path of the machine. This consistency is achieved by removing the second row of blades from the tandem blade diffuser and adjusting the angular distribution of the return channel blades, resulting in an optimized structure (Opt) surpassing the original structure (Ori). The original structure comprises a tandem diffuser and a matching return channel. In contrast, the optimized structure comprises a single semi-high diffuser and a matching return channel. However, this performance enhancement is solely validated through numerical simulation, without testing on a rotating test rig.

Initial measurements were conducted on the stationary component test rig. Upon achieving satisfactory results, verification was performed on the rotating test rig. This approach mitigated experimental risk and reduced manufacturing costs. Figure 19 illustrates the structural comparison of the two return ducts pre- and post-optimization. The figure showcases meridional views in the two structures in the upper part and the return channel vanes before and after optimization in the lower section.

The centrifugal compressor stationary component test rig lacks the capability to assess the overall aerodynamic performance of the entire machine, encompassing efficiency and pressure ratio. However, it facilitates quantitative experimental analysis to examine the performance and function of each stationary component. Therefore, the performance of Opt was measured on the stationary component test rig using the same measurement scheme as Ori. Figure 20 depicts the specific and cumulative values of the total pressure loss coefficient and the static pressure recovery coefficient for both structures, the specific coefficient employs the same computation approach as described previously. The accumulated loss coefficient refers to the loss of all components from the MP1 section. MP1-MP3 refers to the total loss of the diffuser and U-bend, MP1-MP4 refers to the total loss of the diffuser, U-bend, return-channel and L-bend. The



(a) Original structure



(b) Optimized structure

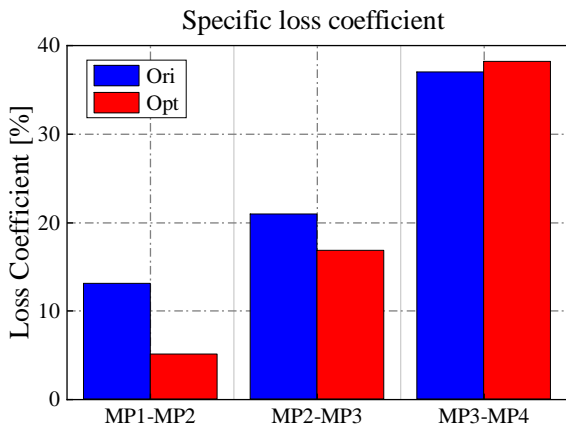
Fig. 19 Comparison of the two return-channel structures

accumulated pressure recovery coefficients are also compared using the same approach.

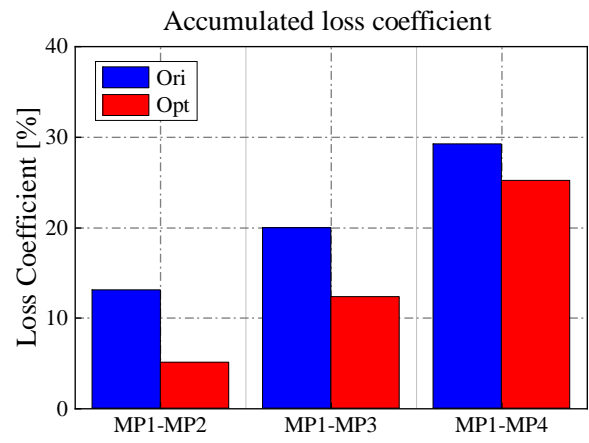
Figure 20(a) showcases that the diffuser of the Opt structure with a single half-height diffuser (MP1–MP2) significantly reduces the pressure loss coefficient (only one-third of that of the Ori structure). In addition, the total pressure loss in the U-bend (MP2–MP3) is reduced by 20%. This trend is also reflected in the circumferentially averaged total pressure distribution in the section (Fig. 21(a)). Compared to the tandem blade diffuser, the single half-height blade diffuser significantly enhances the internal flow of the high flow coefficient compressor, mitigating losses and augmenting efficiency.

In the return channel (MP3–MP4), the specific loss coefficient of the Opt structure is higher than that of the Ori structure. This is due to the fact that the Mach number and airflow angle distribution of the MP3 in the Opt structure is higher than that of the Ori structure (Fig. 21(c) and 21(d)). The high-speed flow with a high flow incidence angle will result in greater losses in the return channel, as evidenced by the total pressure distribution curve, which is a consequence of the return channel structure.

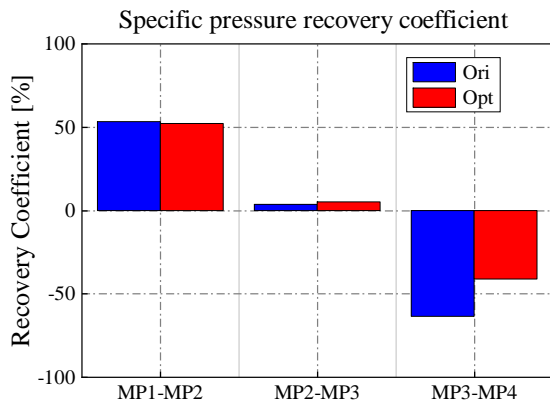
Figure 20(c) illustrates the static pressure recovery of each component. The static pressure recovery coefficients of the diffuser and the U-bend in both structures are closely aligned. This correlation is also reflected in the static pressure curve (Fig. 21(b)), where the static pressures at the MP2 and MP3 of both structures exhibit parallel distribution patterns with consistent variation trends. However, the static pressure recovery coefficient of the Opt structure in the return channel significantly



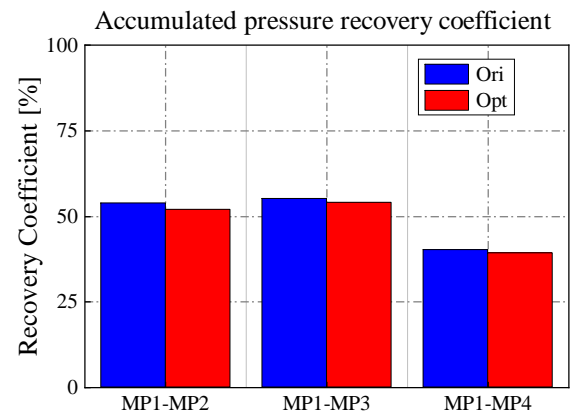
(a) Specific loss coefficient



(b) Accumulated loss coefficient

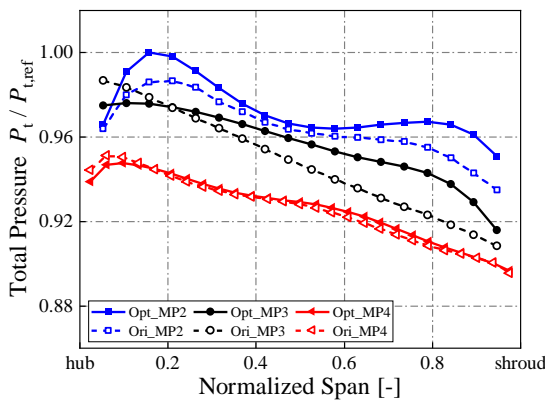


(c) Specific pressure recovery coefficient

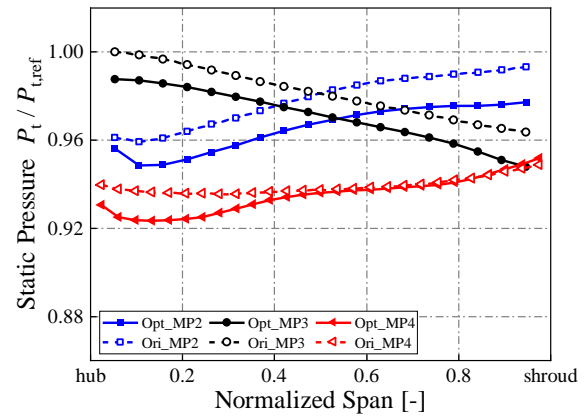


(d) Accumulated pressure recovery coefficient

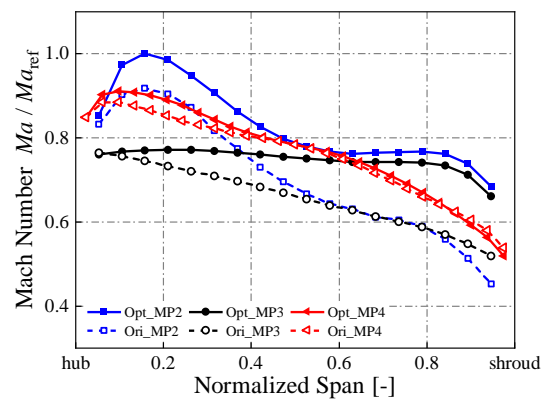
Fig. 20 Performance comparison of stationary components with two different structures



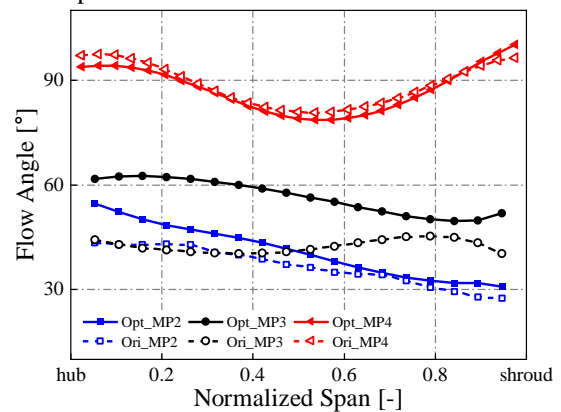
(a) Total pressure



(b) Static pressure

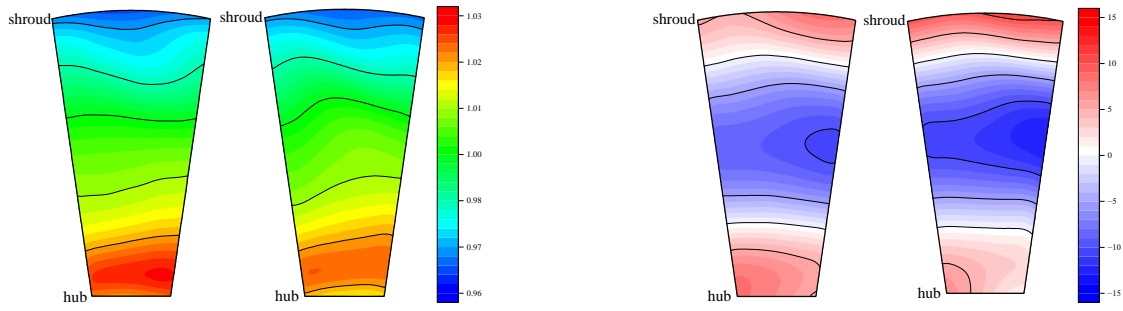


(c) Mach number



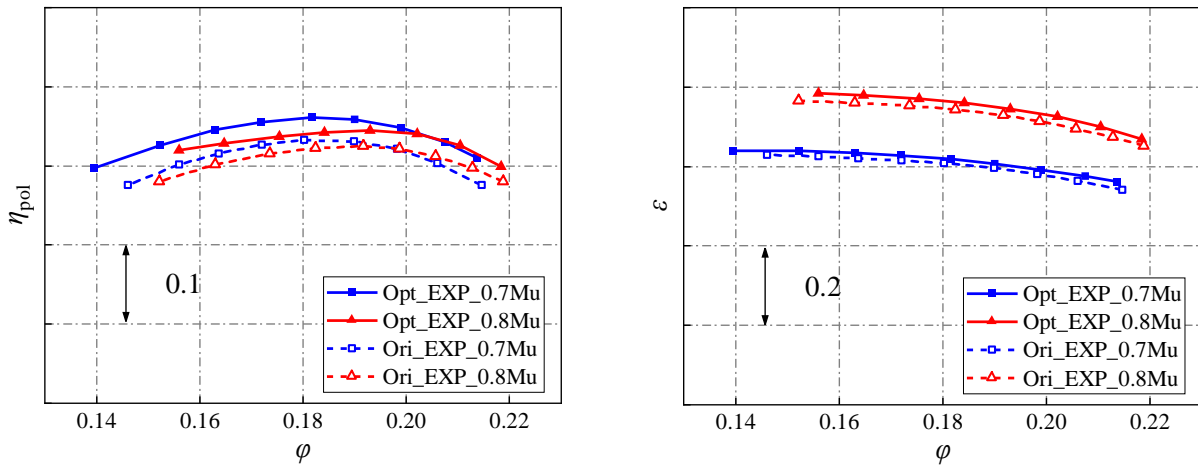
(d) Flow angle

Fig. 21 Comparison of experimental results of the two structures



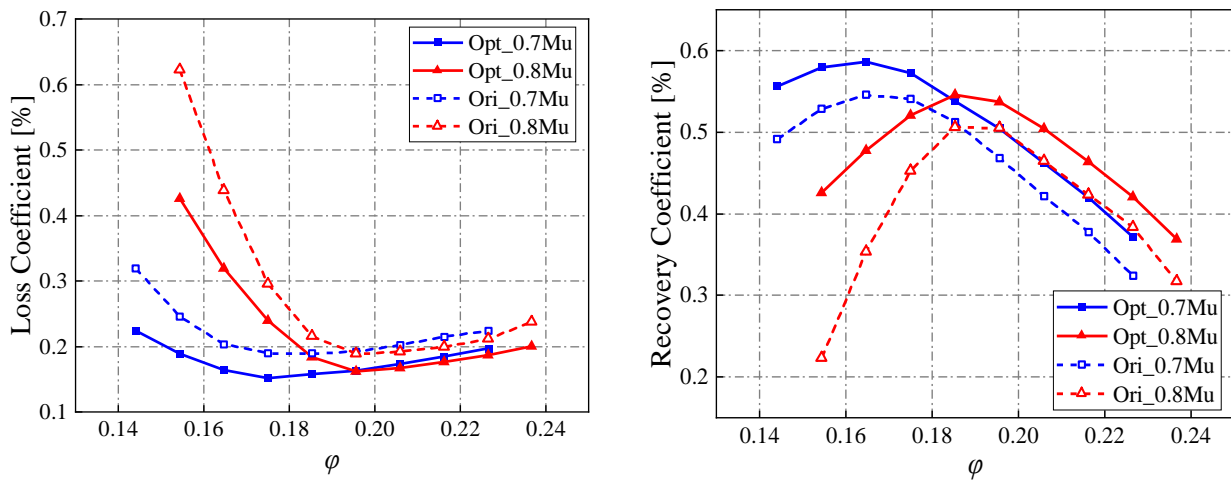
(a) Total Pressure (left: Ori, right: Opt) (b) Flow Angle (left: Ori, right: Opt)

Fig. 22 Comparative analysis of outlet flow fields of the two structures



(a) Polytropic efficiency (b) Pressure ratio

Fig. 23 Comparative analysis of variable working condition performance of the two structures (results of rotational experiment)



(a) Total pressure loss coefficient (b) Static pressure recovery coefficient

Fig. 23 Comparative analysis of numerical calculation results of the stationary component performance of the two structures (MP1–MP4)

decreases, consistent with the variation trend of the total pressure loss coefficient. The static pressure distribution curve of the MP4 section (Fig. 21(b)) indicates a considerable decrease in the static pressure of the Opt structure near the hub at 40% blade height, attributed to the high Mach number and large flow angle at the MP3. Figures 20(b) and 20(d) reveal a 4% reduction in the total pressure loss coefficient of the optimized structure, with a

1% increase in the static pressure recovery coefficient.

Figure 21 shows a comparison of parameters across three measurement planes. Substantial disparities are observed between parameters in MP2 and MP3, while the differences in MP4 (stage exit plane) are insignificant. Variations in MP2 and MP3 stem from distinct diffuser structures. Optimization of the structure has led to a more uniform velocity distribution and a flow angle distribution

closer to the geometric angle at the blade inlet in the return channel inlet plane (MP3) compared to the Ori structure

Figure 22 shows the experimental measurements of the total pressure contour and flow angle contour of the MP4 plane of both structures. The distribution patterns of the two structures are similar with no significant differences. However, the performance of the Opt structure notably surpasses that of the Ori structure. Therefore, when analyzing and optimizing stationary components, it is crucial to consider the differences in the outlet section and variations in each section within the return channel.

The optimized model was experimentally tested on the model scale test rig of Shenyang Blower Group Co., Ltd. (Fig. 23), revealing enhancements in pressure ratio and efficiency. The efficiency and pressure ratio exhibit an average increase of 2.9% and 1.4% at $\text{Mu}=0.8$, respectively, while at $\text{Mu}=0.7$, the efficiency and pressure ratio exhibit an average increase of 3.4% and 0.9%, respectively. However, due to the space and safety limitations of the rotary test bench, only the measuring probe is arranged in the inlet and outlet section of the compressor. Consequently, only the external characteristic curve of the entire machine can be obtained. This limitation of the rotating bench can be overcome on the stationary unit bench.

The variable operating condition performance of the stationary component can solely be acquired through numerical simulation during the existing rotating test (Fig. 24). The figure illustrates the overall aerodynamic performance of the static components of both structures (MP1–MP4), encompassing the total pressure loss coefficient and the static pressure recovery coefficient. A substantial enhancement of the internal loss of the static component is evident post-optimization, affirming the accuracy and feasibility of measuring the static component's performance on the test rig (Fig. 20).

6. CONCLUSIONS

This study presents the design methodology and application of a stationary component test rig for centrifugal compressors. The following conclusions can be drawn.

1. Specially designed stationary vanes replace the impeller to simulate the impeller outlet flow field. Experimental results show that the average outlet circumferential flow angle and Mach number of the stationary vanes are consistent with those of the rotating impeller, confirming the feasibility of the proposed approach.

2. Simulation of impeller rotation is achieved by adjusting the relative position between the stationary vanes and the diffuser. The flow fields measured in each section correspond to those at a specific moment in the actual flow. This mechanism allows the flow of the stationary components of the centrifugal compressor to be studied at that moment, which is impossible with a rotating test rig.

3. An improved diffuser and return channel of the

same centrifugal compressor model stage is tested on the stationary component test rig. The experimental results show a 4% reduction in the total pressure loss coefficient and a 1% increase in the static pressure recovery coefficient compared to the original structure. These results are consistent with those obtained on a rotating test rig and indicate the feasibility of the proposed stationary component aerodynamic performance test rig.

ACKNOWLEDGMENTS

The authors would like to thank Shenyang Blower Group Co., Ltd for funding this work.

CONFLICT OF INTEREST

The authors have no conflicts of interest.

AUTHORS' CONTRIBUTION

K. Zhao: Conceptualization, Methodology, Validation, Writing—review & editing, software. **Y. Liu:** Methodology, Writing—review & editing. **Y. Zhang:** Methodology, Writing—review & editing. **X. Liu:** Experimental measurement. **H. Shi:** Experimental measurement.

REFERENCES

- Aalburg, C., Sezal, I., Haigermoser, C., Simpson, A., Michelassi, V., & Sassanelli, G. (2011). *Annular cascade for radial compressor development*. Turbo Expo: Power for Land, Sea, and Air. <https://doi.org/10.1115/GT2011-46834>
- Aalburg, C., Simpson, A., Schmitz, M., Michelassi, V., Evangelisti, S., Belardini, E., & Ballarini, V. (2008). *Design and testing of multistage centrifugal compressors with small diffusion ratios*. Turbo Expo: Power for Land, Sea, and Air. <https://doi.org/10.1115/GT2008-51263>
- Dolle, B., Brillert, D., Dohmen, H., & Benra, F. K. (2019). *Experimental and numerical investigation on the flow in a return channel of multistage centrifugal compressors*. Turbo Expo: Power for Land, Sea, and Air. <https://doi.org/10.1115/GT2019-90455>
- Ferrara, G., Ferrari, L., & Baldassarre, L. (2004). *Low solidity vaned diffusers for rotating stall prevention: Experimental analysis of some design parameters*. Turbo Expo: Power for Land, Sea, and Air. <https://doi.org/10.1115/GT2004-54146>
- Gilarranz R, J. L., Lombardi, L. M., Keesler, J. E., Maier, W. C., Koch, J. M., & Sorokes, J. M. (2009). Actuation and control of a moveable geometry system for a full-scale, multi-stage centrifugal compressor test vehicle. Turbo Expo: Power for Land, Sea, and Air. <https://doi.org/10.1115/GT2009-60310>
- Hildebrandt, A. (2011). *Aerodynamic optimisation of a centrifugal compressor return channel and U-turn with genetic algorithms*. Turbo Expo: Power for

- Land, Sea, and Air. <https://doi.org/10.1115/GT2011-45076>
- Lenke, L., & Simon, H. (1999). *Numerical investigations on the optimum design of return channels of multi-stage centrifugal compressors*. Turbo Expo: Power for Land, Sea, and Air. <https://doi.org/10.1115/99-GT-103>
- Li, S., Liu, Y., Li, H., & Omid, M. J. A. S. (2021). Numerical study of the improvement in stability and performance by use of a partial vaned diffuser for a centrifugal compressor stage. *Applied Sciences*, 11(15), 6980. <https://doi.org/10.3390/app11156980>
- Oh, J. M., Engeda, A., & Chung, M. K. (2005). A numerical study of the U-turn bend in return channel systems for multistage centrifugal compressors. *Proceedings of the Institution of Mechanical Engineers, Part C: Journal of Mechanical Engineering Science*, 219(8), 749-756. <https://doi.org/10.1243/095440605X31760>
- Rube, C., Rossbach, T., Wedeking, M., Grates, D., & Jeschke, P. (2016). Experimental and numerical investigation of the flow inside the return channel of a centrifugal process compressor. *Journal of Turbomachinery*, 138(10), 101006. <https://doi.org/10.1115/1.4032905>
- Seki, W., Ueda, K., Shirakata, Y., Fukushima, R., Mori, K., & Koga, J. (2006). New model turbo chiller, AART Series, contributes to the reduction of energy consumption under year-run operation. *Mitsubishi Heavy Industries Technical Review*, 43, 1-5. <https://citeseerx.ist.psu.edu/document?repid=rep1&type=pdf&doi=ed203b6a68be92df5e3000314c9a71b29797a159>
- Simpson, A., Aalburg, C., Schmitz, M. B., Pannekeet, R., Michelassi, V., & Larisch, F. (2014). Application of flow control in a novel sector test rig. *Journal of Turbomachinery*, 136(4), 041002. <https://doi.org/10.1115/GT2009-60126>
- Simpson, A., Aalburg, C., Schmitz, M., Pannekeet, R., Larisch, F., & Michelassi, V. (2008). *Design, validation and application of a radial cascade for centrifugal compressors*. Turbo Expo: Power for Land, Sea, and Air. <https://doi.org/10.1115/GT2008-51262>
- Sorokes, J. M. (2013). *Range versus Efficiency-striking the proper balance*. Proceedings of the 42nd Turbomachinery Symposium. <https://doi.org/10.21423/R1BP89>
- Xi, G., Tian, Y., Guo, Y., Tang, Y., & Wang, Z. (2019). *Experimental and numerical investigations on flow losses of a u-bend and return channel system for centrifugal compressor*. Turbo Expo: Power for Land, Sea, and Air. <https://doi.org/10.1115/GT2019-90559>
- Yagi, M., Nishioka, T., Kobayashi, H., Nishida, H., & Yamamoto, S. (2015). *Effects of return channel with splitter vanes on performance of multistage centrifugal compressor*. Turbo Expo: Power for Land, Sea, and Air. <https://doi.org/10.1115/GT2015-42442>
- Zhao, P. F., Liu, Y., & Wang, X. F. (2017). Analysis of vortices and performance of different diffusers in a large mass flow coefficient centrifugal compressor. *Proceedings of the Institution of Mechanical Engineers, Part A: Journal of Power and Energy*, 231(4), 253-273. <https://doi.org/10.1177/0957650917701339>